JOURNAL OF CATALYSIS 142, 585–601 (1993)

Iridium Clusters in NaX Zeolite Cages: Synthesis, Characterization, and Selective Catalysis of CO Hydrogenation

S. KAWI, J.-R. CHANG, AND B. C. GATES[1]

Center for Catalytic Science and Technology, Department of Chemical Engineering, University of Delaware, Newark, Delaware 19716

Received January 4, 1993; revised April 5, 1993

[$Ir(CO)_2$(acac)] in the pores of NaX zeolite was treated in CO at 1 atm and various temperatures and characterized by infrared and extended X-ray absorption fine structure (EXAFS) spectroscopies. The iridium precursor was converted predominantly into $[HIr_4(CO)_{11}]^-$ at 70°C, and predominantly into $[Ir_6(CO)_{15}]^{2-}$ at 175°C, as indicated by infrared spectra. The infrared spectra indicate that both of these clusters interact through ion pairing with the zeolite support. The chemistry of their synthesis in the zeolite cages parallels that on the basic MgO surface and in basic solutions. The zeolite-supported samples catalyzed CO hydrogenation at 20 atm and 250°C, having a relatively low activity in comparison with those of typical Fischer–Tropsch catalysts. The catalyst gave a non-Schulz–Flory distribution of hydrocarbon products with a maximum at C_1 and a relative maximum at C_4. Infrared and EXAFS spectra of the catalyst used with equimolar CO + H_2 feed showed that the predominant iridium-containing species was $[Ir_6(CO)_{15}]^{2-}$.

INTRODUCTION

In the early 1970s, the chemistry of metal carbonyl clusters was emerging from its infancy, and in 1975, Muetterties (*1*) discussed analogies between metal clusters and metal surfaces and speculated that molecular metal clusters would be found to be catalysts with novel properties. However, only a few reactions catalyzed by metal clusters have been discovered (*2*), and the clusters appear to be limited by their fragility. One of the potential cluster-catalyzed reactions was recognized to be CO hydrogenation, as CO and H are common ligands in metal clusters and may help to stabilize them (*3*), and thus it is appealing (*4*) to investigate metal carbonyl clusters with robust metal frames stabilized by CO ligands as potential CO hydrogenation catalysts. Some of the most robust metal carbonyl clusters are Os and Ir clusters (*3*, *5*).

Solid supports appear to stabilize some metal carbonyl clusters, especially anions (*4*, *5*), and zeolites appear to be especially appropriate, perhaps because the molecular-scale cages help to stabilize the clusters. Carbonyl clusters of Os (*6*, *7*), Rh (*8*), and Ir (*9–11*), for example, have been synthesized in the supercages of faujasites, and they appear to be stabilized by CO and by confinement in the cages. These materials are selective but relatively inactive catalysts for CO hydrogenation, giving non-Schulz–Flory distributions of hydrocarbon products (*6–11*); they are also potential shape-selective catalysts for other reactions, such as olefin hydroformylation (*12*).

Here we report the synthesis, characterization, and catalytic performance of iridium carbonyl clusters formed from [$Ir(CO)_2$(acac)] in NaX zeolite cages. NaX zeolite was chosen because it is moderately basic, and the synthesis of iridium carbonyl cluster anions occurs in basic solutions (*13–17*). This zeolite has been used as a support for rhodium carbonyl clusters (with unidentified structures) that appear to catalyze olefin hydroformylation (*18*). [$Ir(CO)_2$(acac)] was chosen as the catalyst precursor because it offers the following advantages: (1) it has no chloride or other

[1] To whom correspondence should be addressed.

0021-9517/93 $5.00

components that are expected to be catalyst poisons; (2) it is small enough to diffuse readily into the zeolite channels; and (3) it is converted into iridium carbonyl clusters on MgO and γ-Al_2O_3 surfaces in relatively well understood chemistry (*19*, *20*). The iridium-containing species in the zeolite have been characterized by extended X-ray absorption fine structure (EXAFS) spectroscopy and infrared spectroscopy.

EXPERIMENTAL

Materials and Sample Preparation

Synthesis of the zeolite-supported iridium carbonyls was performed with samples in a Braun MB-150M glovebox that was purged with N_2 that recirculated through O_2- and moisture-scavenging traps or on a Schlenk vacuum line that was purged with N_2 (99.999%). The glovebox was equipped with O_2 and moisture detectors that consistently indicated concentrations of these contaminants that were <1 ppm. NaX zeolite powder (Union Carbide, Linde type 13X) had a silica/alumina molar ratio of about 2.5. Prior to preparation of the supported samples, the zeolite was evacuated at 10^{-3} Torr at room temperature for 2 h, but it was not rigorously dried. $[Ir(CO)_2(acac)]$ (Strem) was used without purification. Reagent grade mixed hexanes were purged with N_2 for several hours before use as a solvent. He and H_2 (Matheson, 99.999%) were purified by passage through traps containing particles of Cu_2O and particles of activated zeolite 4A to remove traces of O_2 and moisture, respectively. CO (Matheson, UHP grade) was purified by passage through a trap containing particles of activated γ-Al_2O_3 heated to a temperature exceeding 250°C to remove traces of metal carbonyls from the high-pressure gas cylinder and through a trap containing particles of activated zeolite 4A to remove moisture.

In the preparation of the zeolite-supported Ir-containing samples, $[Ir(CO)_2(acac)]$ (30 mg/g of zeolite, used to make a sample containing 0.8 wt% Ir) was dissolved in hexanes and brought in contact with the preevacuated zeolite. The light-brown NaX zeolite powder became dark brownish green, and the initially greenish-black solution became clearer after stirring for several hours. After 2 days of stirring, the uptake of $[Ir(CO)_2(acac)]$ was complete; the hexane solution was clear and no $[Ir(CO)_2(acac)]$ was detected in the supernatant solution by infrared spectroscopy. The metal-containing zeolite was separated by filtration, washed thoroughly with hexane, and dried under vacuum at room temperature for 12 h. The samples were stored in the glovebox.

Attempts to extract organometallic species from the zeolite were carried out with tetrahydrofuran (THF) (Aldrich) and with bis(triphenylphosphine)iminium chloride ([PPN][Cl]) (Aldrich) dissolved in THF.

Infrared Spectroscopy

Transmission infrared spectra of the zeolite samples were recorded with a Nicolet 7199 FTIR spectrometer with a resolution of 4 cm^{-1}. Samples in the glovebox were pressed into semitransparent wafers and mounted in the infrared cell. The spectra were recorded with the samples in controlled atmospheres; purified He, N_2, CO, or H_2 could be delivered to the cell, which was part of a flow system. A typical gas flow rate was 20–30 ml(NTP)/min. Samples were scanned 32 or more times and the data averaged.

Catalytic Hydrogenation of CO

CO hydrogenation kinetics measurements were made with a copper-lined stainless-steel tubular flow reactor having an inner diameter of $\frac{1}{4}$ in. Typically, 1.0 g of catalyst in the glovebox was loaded into the central (isothermal) zone of the reactor; the upstream and downstream reactor sections were packed with glass wool. The gases used as feeds to the reactor, CO (Matheson, UHP grade) and H_2 (Matheson, UHP grade), passed through a trap containing

particles of activated 4A zeolite; H_2 also flowed through a trap containing particles of Cu_2O to remove residual O_2. CO also flowed through a trap containing particles of activated carbon at 300°C to remove residual metal carbonyls. The reactor was first pressurized in CO + H_2 (equimolar) to 20 atm. The sample in flowing CO + H_2 [12 mL(NTP)/min] was then heated at a rate of 2.5°C/min to 250°C. Time zero on stream was defined as the time when this temperature was reached. The effluent stream flowed through a heated line (held at ca. 140°C) to prevent condensation of products, which were sampled periodically for analysis in an Antek 300 gas chromatograph equipped with a flame ionization detector. The products were separated in a Porapak Q column (4 ft long and $\frac{1}{8}$ in. inside diameter) in a temperature-programmed mode with the column heated at a rate of 4°C/min from 85 to 125°C and held at 125°C for 50 min. The C_1–C_5 hydrocarbon (paraffin and olefin) as well as oxygenate (methanol, ethanol, and dimethyl ether) products were identified and quantified by use of calibration gas mixtures. Measurements of CO_2 and water were not made. Conversions (<2%) were measured as a function of time on stream to provide data characterizing catalyst deactivation. At the conclusion of each experiment, the catalyst was cooled to room temperature in flowing CO + H_2 (equimolar), and the pressure was decreased to 1 atm. The reactor was then sealed, removed from the flow system without contacting of the catalyst with air, and unloaded in the glovebox.

Extended X-Ray Absorption Fine Structure (EXAFS) Spectroscopy

A used catalyst sample was characterized by EXAFS spectroscopy. The experiments were performed on X-ray beamline X-11A at the National Synchrotron Light Source at Brookhaven National Laboratory, Upton, Long Island, New York. The ring energy was 2.5 GeV and the ring current 80–220 mA. The spectra were recorded with the sample in a cell that allowed treatment in flowing gases prior to the measurements. The powder samples were pressed into wafers with a C-clamp inside a glovebag purged with N_2 boiloff gas from a liquid nitrogen cylinder. The amount of sample in a wafer (approximately 150 mg) was calculated to give an absorbance of 2.5 at the Ir L_{III} absorption edge. After the sample had been pressed, it was unloaded from the die and loaded into the EXAFS cell. The cell was then sealed under a positive pressure of N_2, removed from the glovebag, aligned in the X-ray beam, and cooled with liquid nitrogen. The EXAFS data were recorded in the transmission mode after the cells had been cooled to approximately liquid nitrogen temperature. The data were collected with a Si(111) double crystal monochromator that was detuned by 30% to minimize the effects of higher harmonics in the X-ray beam. The sample was scanned at energies near the Ir L_{III} absorption edge (11,215 eV).

The sample characterized by EXAFS spectroscopy was a used catalyst that had been prepared by treating the [Ir $(CO)_2$(acac)]-containing NaX zeolite in the catalytic flow reactor that was fed with equimolar CO + H_2 at 250°C and 20 atm; the catalyst was on stream for 24 h. The catalyst was removed from the sealed reactor inside the glovebox. It was stored in three layers of glass vials that were sealed with parafilm. The sealed sample was transported to the synchrotron, where it was pressed into a wafer and loaded into the EXAFS cell.

EXAFS Reference Data

The EXAFS data were analyzed with experimentally determined reference files obtained from EXAFS data for materials of known structure. The Ir–Ir and Ir–$O_{support}$ (where $O_{support}$ denotes oxygen of the zeolite lattice) interactions were analyzed with phase shifts and backscattering amplitudes obtained from EXAFS data, reported elsewhere (*21*), for Pt foil and $Na_2Pt(OH)_6$, re-

TABLE 1

Crystallographic Data Characterizing the Reference Compounds and Fourier Transform Ranges Used in the EXAFS Analysis[a]

	Crystallographic data			*Fourier transform*		
Sample	Shell	N	R (Å)	Δk (Å^{-1})	Δr (Å)	n
Pt foil	Pt–Pt[b]	12	2.77	1.9–19.8	1.9–3.0	3
$Na_2Pt(OH)_6$	Pt–O[c]	6	2.05	1.4–17.7	0.5–2.0	3
$[Ir_4(CO)_{12}]$	Ir–C[d]	3	1.87	2.8–16.5	1.1–2.0	3
	Ir–O*[d]	3	3.01	2.8–16.5	2.0–3.3	3

[a] Notation: N, coordination number for absorber-backscatterer pair; R, radial distance from crystal structure data; Δk, limits used for forward Fourier transformation (k is the wave vector); Δr, limits used for shell isolation (r is distance); n, power of k used for Fourier transformation.

[b] Crystal structure data from Ref. (*26*).

[c] Crystal structure data from Ref. (*27*).

[d] Crystal structure data from Ref. (*28*); after subtraction of the Ir–Ir contribution: $N = 6$, $R = 2.69$ Å, $\Delta\sigma^2 = -0.001$ Å^2, and $\Delta E_0 = 2.5$ eV.

spectively. The transferability of the Pt and Ir phase shifts and backscattering amplitudes is justified by experimental (*22*) and theoretical results (*23*). The Ir–C and Ir–O* interactions (where O* denotes the oxygen of a carbonyl ligand) were analyzed with phase shifts and backscattering amplitudes obtained from EXAFS data for crystalline $[Ir_4(CO)_{12}]$ (which has only terminal CO ligands) that was mixed with SiO_2. $[Ir_4(CO)_{12}]$ is a good reference material because the multiple scattering effect in the Ir–O* shell is significant (because of the near linearity of the Ir–C–O moiety), and it was necessary to fit with a reference that exhibits multiple scattering (*24*). The details of the preparation of the reference files are described elsewhere (*25*). The EXAFS parameters characteristic of the reference compounds are summarized in Table 1.

RESULTS

Reactivity of [Ir(CO)$_2$(acac)] in NaX Zeolite in the Presence of CO at 1 atm

The infrared spectrum of the freshly prepared [Ir(CO)$_2$(acac)]-containing zeolite (a brownish yellow solid) (Fig. 1A) includes ν_{CO} bands at 2082 s and 1984 s cm^{-1}, indicating the presence of an iridium dicarbonyl species. This sample was exposed to flowing CO at 1 atm. After about 8 h at 75°C, a new spectrum was observed (Fig. 1B), including ν_{CO} bands at 2072 w, 2044 sh, 2035 s, 2011 m, 2000 sh, and 1765 mw cm^{-1}. This spectrum closely resembles that of $[HIr_4(CO)_{11}]^-$ supported on MgO, which has been characterized by infrared and EXAFS spectroscopies and by extraction into solution with [PPN][Cl] in THF (*19, 29*). The ν_{CO} infrared spectra of the supported species resemble those of the salts $[NBu_4][HIr_4(CO)_{11}]$ (*13*) and $[P(CH_2C_6H_5)_3][HIr_4(CO)_{11}]$ (*16*) dissolved in THF (Table 2), except that the major terminal band is shifted about 20 cm^{-1} to higher wavenumbers, and the bridging band is shifted about 60 cm^{-1} to lower wavenumbers, consistent with well-known ion-pairing effects (*19, 30*).

The wafer sample was unloaded in the glovebox; it was light yellow, the color of $[NBu_4][HIr_4(CO)_{11}]$ in THF solution. Attempts were made to extract the iridium carbonyl species from the zeolite to allow a comparison of its infrared spectrum with that of $[NBu_4][HIr_4(CO)_{11}]$ in solution. However, the extractions, which were at-

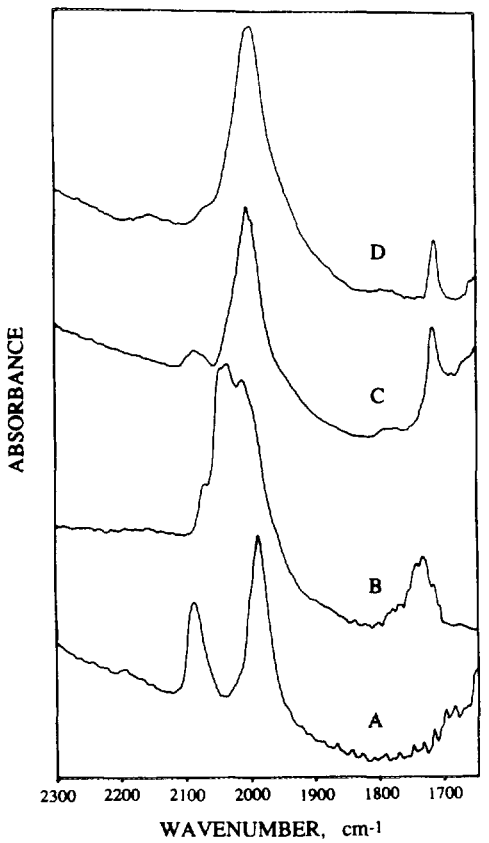

FIG. 1. Infrared spectra taken during treatment of the initially prepared sample made from [Ir(CO)$_2$(acac)] and NaX zeolite: (A) [Ir(CO)$_2$(acac)] adsorbed in NaX zeolite, (B) after treatment in CO at 75°C for 8 h, (C) after treatment in CO at 175°C for 2 h, and (D) used CO hydrogenation catalyst after exposure to equimolar CO + H_2 at 20 atm and 250°C for 3 days.

tempted under N_2 in the glovebox with THF and, alternatively, with a solution of excess [PPN][Cl] in THF, were unsuccessful. In contrast to the results reported for the MgO-supported $[HIr_4(CO)_{11}]^-$ (*19*), the zeolite wafer remained light yellow after the extraction attempt, while the solution remained colorless. No carbonyls were observed in the supernatant solution by infrared spectroscopy, indicating that no such species were extracted from the zeolite. These results are consistent with the entrapment of the iridium carbonyl species in the zeolite pores.

In another experiment, a new wafer of a zeolite-supported sample prepared from [Ir(CO)$_2$(acac)] was loaded into the infrared cell. It was treated in flowing CO at 75°C for 8 h to form $[HIr_4(CO)_{11}]^-$, as described above. The temperature was then raised to 150°C, and after 2 h a new spectrum (ν_{CO}: 2001 s, 1993 s, 1710 m cm^{-1}) was observed (Fig. 1C). This spectrum is almost the same as that of $[Ir_6(CO)_{15}]^{2-}$ supported on MgO (Table 2), which has been characterized by infrared and EXAFS spectroscopies and by extraction with [PPN][Cl] in THF solution (*19, 31*). The spectra of the supported clusters in the zeolite and on MgO (*19, 31*) resemble that of $[NMe_4]_2[Ir_6(CO)_{15}]$ (*13*) and that of $[NMe_3CH_2Ph]_2[Ir_6(CO)_{15}]$ (*14*) in THF solution (Table 2), except that the major terminal CO bands of the supported clusters are shifted about 12 cm^{-1} to higher frequency and those of the bridging ligands are shifted about 60 cm^{-1} to lower frequency relative to those of the cluster in solution. Again, the comparison indicates ion-pairing effects (*17, 19, 31*).

The wafer unloaded in the glovebox was light reddish brown. Again, extraction of the surface species from the zeolite was attempted with THF and with [PPN][Cl] in THF. The wafer remained reddish brown after the extraction attempts, while the solution remained colorless. Moreover, no carbonyls were detected in the extract solution with infrared spectroscopy, which indicates that no iridium carbonyls were extracted from the zeolite, presumably because they remained trapped in it.

Catalytic Hydrogenation of CO

The iridium-containing zeolite was found to catalyze CO hydrogenation at temperatures of 225°C and greater. Conversions were measured as a function of time on stream in the flow reactor. Catalytic activities are represented as rates of reaction calculated from differential conversion data and are expressed in units of [mol of CO

TABLE 2

Infrared Spectral Data in the Carbonyl Stretching Region Characterizing NaX-Supported Iridium Carbonyl Species and Related Molecular Iridium Clusters

Sample	ν_{CO} (cm^{-1})	Reference
$[Ir(CO)_2(acac)]$ in NaX (1A)	2082 s, 1984 s	This work
1A, then CO at 75°C, 8 h (1B)	2072 w, 2044 sh, 2035 s, 2011 m, 2000 sh, 1765 mw	This work
1B, then CO at 175°C, 2 h	2001 s, 1993 s, 1710 m	This work
$[NEt_4][HIr_4(CO)_{11}]$ in THF	2067 w, 2030 sh, 2017 vs, 1986 m, 1978 m, 1832 m	(*30*)
$Na[HIr_4(CO)_{11}]$ in diethyl ether	2072 w, 2039 s, 2020 vs, 1990 m, 1984 m, 1830 w, 1730 m	(*30*)
$[P(CH_2C_6H_5)(C_6H_5)_3]$-$[HIr_4(CO)_{11}]$ in THF	2015 vs, 2005 vs, 1985 s, 1970 s, 1800 m	(*16*)
$[NMe_4]_2[Ir_6(CO)_{15}]$ in THF	2030 sh, 1970 s, 1910 sh, 1775 s, 1735 s	(*13*)
$Na_2[Ir_6(CO)_{15}]$ in THF	1993 s, 1984 s, 1928 w, 1788 m, 1735 m	(*31*)

converted to hydrocarbons (mol of total Ir · s)$^{-1}$]. All the catalysis experiments reported here were conducted for CO conversions between 0.1 and 2.0%. The standard conditions were chosen to be 250°C, 20 atm, space velocity = 20 [mL (NTP) (g of catalyst · min)$^{-1}$], and CO/H_2 feed molar ratio = 1.0. A blank experiment was performed with the reactor packed with NaX zeolite in the absence of iridium; no conversion was observed under the standard operating conditions.

The product distribution observed with the zeolite-supported catalyst that was on stream for 3 days is shown in Fig. 2. The catalyst gave relatively high yields of C_2–C_4 hydrocarbons with high olefin selectivity. Products with chain lengths >5 were formed in only very low yields at the low conversions observed (typically, 0.3%).

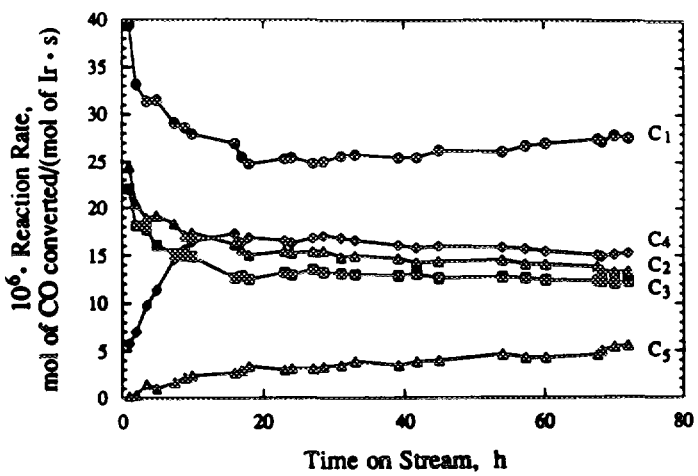

FIG. 2. CO hydrogenation catalyzed by zeolite-supported iridium carbonyl clusters: dependence of product distribution on time on stream in a flow reactor up to 3 days. Reaction conditions: 250°C, 20 atm, CO/H_2 = 1.0 (molar).

The catalyst showed major changes in product distribution during the first 15 h on stream; most notable was the increased rate of formation of C_4 products, the yields of which became higher than those of C_2 products. After 15 h, the selectivity changed only slightly with time on stream in the flow reactor.

The peaks in the chromatograms characterizing the C_4 products were not always well resolved. When they were, selectivities to the various butene and butane isomers were determined. The data show that the ratio of iso to normal C_4 products was in the range 0.2–0.3.

The hydrocarbon product distribution after 1 day on stream is shown in the Schulz–Flory plot of Fig. 3. A substantial deviation from linearity is evident, with a relative maximum at C_4. The major product was methane. This product distribution did not change substantially with time on stream in the flow reactor, as shown in Figs. 2 and 3. The catalyst removed from the reactor after either two or three days was reddish brown.

A few experiments were done to determine the effects of space velocity, pressure, and feed composition on catalyst performance. The conversion to hydrocarbons

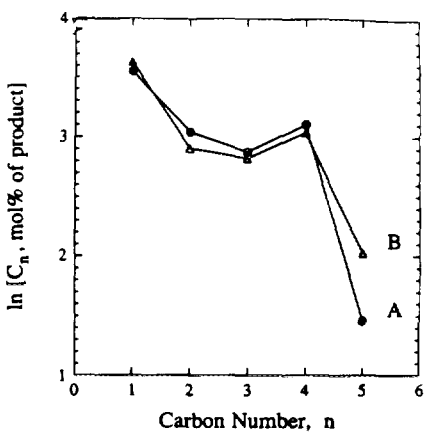

FIG. 3. Hydrocarbon product distributions in CO hydrogenation catalyzed by zeolite-supported iridium carbonyl clusters for (A) 1 day and (B) 3 days on stream.

was observed to be proportional to the inverse space velocity, confirming that the conversions were differential, determining reaction rates directly.

To determine the effect of H_2 partial pressure on catalyst stability, a sample of $[Ir(CO)_2(acac)]$-containing NaX zeolite was treated for 24 h at 250°C and 20 atm in flowing CO/H_2 with a molar ratio of only $\frac{1}{3}$. The activity of the catalyst was then about seven times higher than that observed for the catalyst used in equimolar CO/H_2. The product distribution data (not shown) correspond to the Schulz-Flory distribution. Furthermore, when the catalyst that had been used in CO/H_2 with a molar ratio of $\frac{1}{3}$ was removed from the reactor, the upstream end of the catalyst bed was black, suggesting that Ir metal particles had formed on the zeolite outer surface after treatment at the relatively high H_2 partial pressure.

A pressure of 20 atm was found to be essential for stable catalyst performance when the feed was equimolar CO/H_2. At lower pressures, the catalyst slowly lost activity in operation. After 24 h in operation at only 1 atm and otherwise the standard conditions stated above, the used catalyst removed from the reactor was dark gray, suggesting the formation of Ir metal particles on the outer zeolite surface.

Catalyst Characterization by Infrared Spectroscopy

A sample of catalyst that had been used for CO hydrogenation at 20 atm and 250°C for 3 days was removed from the reactor in the absence of air. The infrared spectrum of the used reddish-brown catalyst is shown in Figure 1D. The spectrum in the ν_{CO} region is almost the same as that of MgO-supported $[Ir_6(CO)_{15}]^{2-}$ (*19, 31*) and that of the zeolite-supported iridium carbonyl prepared by treatment under 1 atm of CO, as described above (Fig. 1C).

Attempts to extract iridium carbonyls from the used catalyst sample with THF or with [PPN][Cl] in THF were unsuccessful.

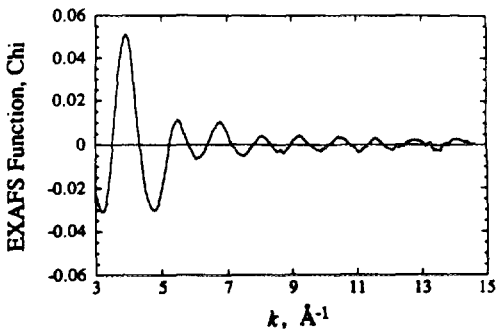

FIG. 4. Raw EXAFS data characterizing the used catalyst of the zeolite-supported Ir carbonyl after exposure to equimolar CO + H_2 at 20 atm and 250°C for 1 day.

The supernatant solutions remained colorless and had no carbonyl absorptions. The result is consistent with the entrapment of iridium carbonyl clusters in the zeolite cages.

Catalyst Characterization by EXAFS Spectroscopy

The catalyst that had been used for CO hydrogenation at 20 atm and 250°C for 24 h with an equimolar CO/H_2 feed was also characterized by EXAFS spectroscopy. The normalized EXAFS function was obtained from the average of the X-ray absorption spectra from three scans by a cubic spline background subtraction and normalized to the height of the absorption edge. The raw EXAFS data (Fig. 4) show oscillations up to a value of k, the wave vector, of about 14 $Å^{-1}$, indicating the presence of near-neighbor high-atomic-weight backscatterers, which are inferred to be Ir. Since the infrared data indicate that carbonyl ligands were also present in the sample, the data were first analyzed for Ir–Ir, Ir–C, and Ir–O* interactions. The EXAFS analysis was done with the experimentally determined reference files described above.

The raw EXAFS data were Fourier transformed with a k^2-weighting over the range $3.54 < k < 13.52$ $Å^{-1}$ with no phase correction. The Fourier-transformed data were then inverse transformed in the range $0.55 < r < 3.47$ Å (where r is distance from the absorbing Ir atom) to isolate the major contributions from low-frequency noise and higher-shell contributions. With the Koningsberger difference file technique (*32*, *33*), the Ir–Ir contribution, the largest in the EXAFS spectrum, was then estimated. Since the Ir–O* contribution was found to be strongly coupled with the Ir–Ir contribution, these two contributions had to be analyzed simultaneously. The structural parameters were estimated initially by fitting the data in the high-k range ($7.0 < k < 13.0$ $Å^{-1}$). The multiple scattering associated with Ir–C–O* groups was found to be significant in this range, with Ir–$O_{support}$ and Ir–C contributions being insignificant.

Further analysis following the subtraction of the calculated Ir–Ir and Ir–O* contributions from the raw data led to characterization of the Ir–C_t and Ir–C_b contributions (where the subscripts t and b refer to terminal and bridging, respectively). The structural parameters characterizing these contributions were determined by fitting the residual spectrum. The initial guesses for parameter estimation were obtained by adjusting the coordination parameters to give the best fit of the residual spectrum in r space. The calculated Ir–C contributions were then subtracted from the raw data. Better parameters for the Ir–Ir and Ir–O* contributions were then estimated by fitting the residual spectrum. The iteration was continued until the best overall agreement was obtained. However, the fit was still not satisfactory, and it was concluded that another backscatterer had to be accounted for. It was postulated to be oxygen of the support, $O_{support}$.

The analysis was repeated as described above, except for the complication of the added backscatterer. Now a satisfactory fit was obtained. The parameters determined in this fitting routine are summarized in Table 3, and the comparisons of the data and the fit, both in k space and in r space, are

TABLE 3

EXAFS Results Characterizing the NaX-Supported Iridium Carbonyl Species Formed after Treatment in Equimolar CO + H_2 at 250°C and 20 atm for 1 Day[a,b]

Shell	N	r (Å)	$\Delta\sigma^2$ (Å^2)	ΔE_0 (eV)	EXAFS reference
Ir–Ir	3.2	2.76	0.0023	2.32	Pt–Pt
Ir–CO					
Ir–C_t	1.3	1.82	0.0032	0.09	Ir–C
Ir–C_b	0.7	1.96	0.0046	−8.60	Ir–C
Ir–O*	1.46	2.99	0.0027	−5.46	Ir–O*
Ir–$O_{support}$	1.45	2.16	0.0065	−7.50	Pt–O

[a] Notation as in Table 1.

[b] Estimated precision: N, ±20% (Ir–$O_{support}$, ±30%); r, ±1% (Ir–O*, Ir–C_t, Ir–C_b, Ir–$O_{support}$, ±2%); $\Delta\sigma^2$, ±30%, ΔE_0, ±10%.

shown in Figs. 5A–5C. The residual spectrum determined by subtracting the Ir–Ir + Ir–$O_{support}$ contributions from the raw data, giving evidence of the carbonyl ligands, is shown in Fig. 5D.

The number of parameters used to fit the data in this main-shell analysis is 20; the statistically justified number is approximately 20. This value was estimated from the Nyquist theorem (*34*), $n = (2\Delta k\Delta r/\pi) + 1$, where Δk and Δr, respectively, are the k and r ranges used in the forward and inverse fourier transforms (Δk = 9.98 Å^{-1}; Δr = 2.92 Å).

DISCUSSION

EXAFS Evidence of $[Ir_6(CO)_{15}]^{2-}$ in NaX Zeolite after Catalysis of CO Hydrogenation

The EXAFS results show that the backscatterers in the immediate vicinity of the Ir absorber atoms in the zeolite-supported iridium catalyst included Ir and low-atomic-weight scatterers identified by the multiple scattering effect as C and O*. These results are consistent with the presence of iridium carbonyl clusters in the zeolite. However, a satisfactory fit was obtained only after inclusion of another low-atomic-weight backscatterer that we suggest to be oxygen of the zeolite support. Since EXAFS cannot usually distinguish one low-atomic-weight backscatterer from another (the multiple scattering effect allows identification of the carbonyl ligands, however), we cannot be highly confident of this last assignment.

The data of Table 3 show that the Ir–Ir interactions are characterized by a first-shell contribution but no higher-shell contributions, consistent with the inference that the clusters were very small. The Ir–Ir first-shell coordination number of 3.4 (with an estimated error of ±20%) suggests the presence of clusters with only 4–6 Ir atoms. The Ir–Ir distance (2.76 Å, with an estimated error or ±1%) is nearly the same as the value for $[N(CH_3)_3CH_2C_6H_5]_2[Ir_6(CO)_{15}]$ in the crystalline state [2.77 Å] (*14*); in contrast, the average Ir–Ir bond distance in $[P(CH_2C_6H_5)(C_6H_5)_3][HIr_4(CO)_{11}]$ in the crystalline state is only 2.73 Å (*16*). (All the Ir atoms in crystalline $[N(CH_3)_3CH_2C_6H_5]_2[Ir_6(CO)_{15}]$ are stereochemically equivalent, with each one bonded to four Ir atoms.) Thus the EXAFS data are consistent with the presence of hexairidium clusters anions in the zeolite, in agreement with the color and the infrared spectra.

Thus the EXAFS data are interpreted as indicating the presence of a mixture of iridium carbonyl clusters and other iridium species that are bonded to the zeolite support, which provides the oxygen ligands. A

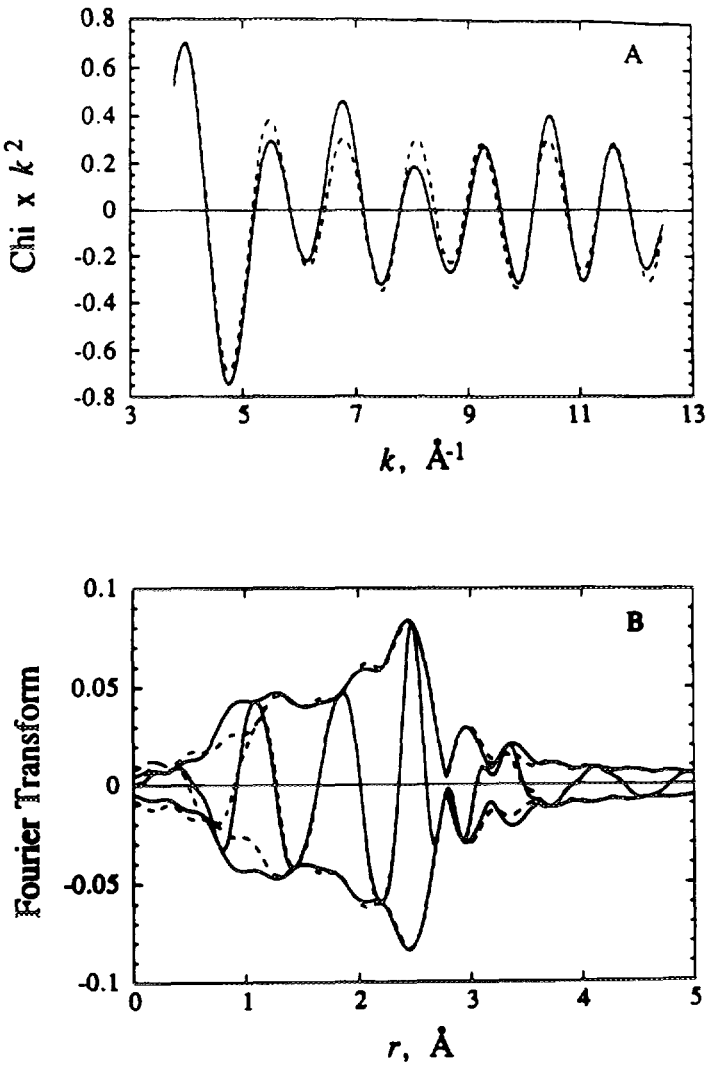

FIG. 5. Results of EXAFS analysis obtained with the best calculated coordination parameters characterizing zeolite-supported Ir carbonyl after exposure to equimolar CO + H_2 at 20 atm and 250°C for 1 day: (A) experimental EXAFS (solid line) and sum of the calculated Ir–Ir + Ir–C_t + Ir–C_b + Ir–$O_{support}$ contributions (dashed line); (B) imaginary part and magnitude of Fourier transform (k^1-weighted, Δk = 3.80–13.0 Å^{-1}) of experimental EXAFS (solid line) and sum of the calculated Ir–Ir + Ir–C_t + Ir–C_b + Ir–O* + Ir–$O_{support}$ contributions (dashed line); (C) imaginary part and magnitude of Fourier transform (k^3-weighted, Δk = 3.80–13.0 Å^{-1}) of experimental EXAFS (solid line) and sum of the calculated Ir–Ir + Ir–C_t + Ir–C_b + Ir–O* + Ir–$O_{support}$ contributions (dashed line); and (D) residual spectrum illustrating the contributions of carbonyl groups: imaginary part and magnitude of Fourier transform (k^3-weighted, Δk = 3.80–13.0 Å^{-1}) of raw data minus calculated Ir–Ir + Ir–$O_{support}$ EXAFS (solid line) and calculated Ir–C_t + Ir–C_b + Ir–O* EXAFS (dashed line).

simple interpretation that is consistent with the data (explaining the Ir–Ir coordination number that is less than four, the value that would be observed for Ir_6 octahedra) is that the minor species present along with the clusters are mononuclear (single-Ir-atom) species such as iridium subcarbonyls; such species have been identified by infrared

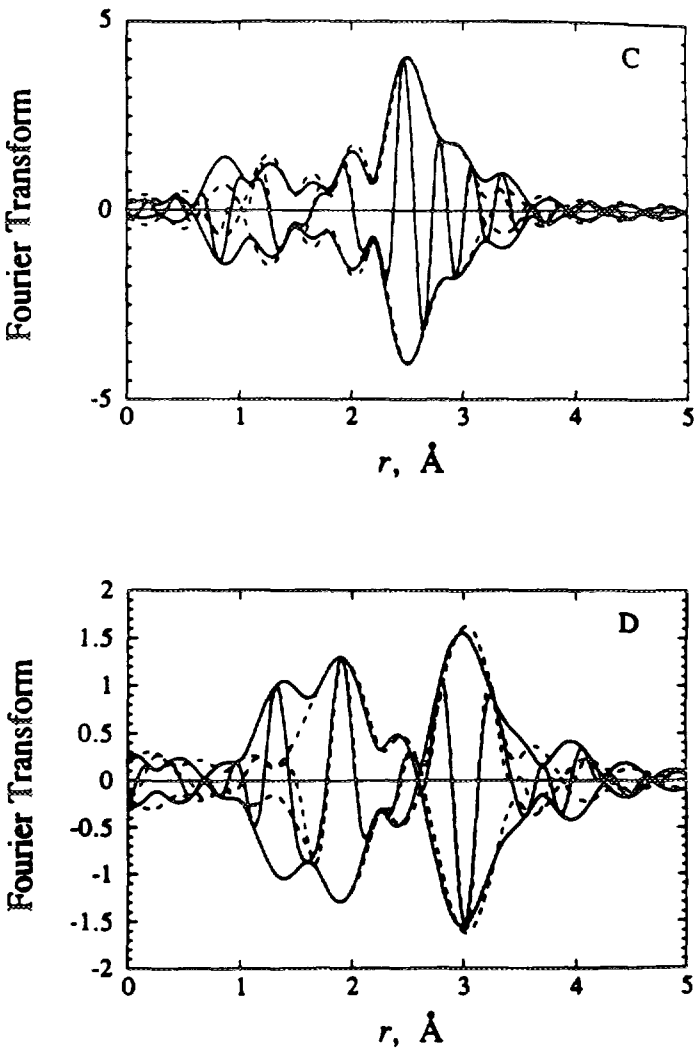

FIG. 5—*Continued*

spectroscopy on the surface of alumina (*20*, *35*, *36*) as well as in NaX (*10*, *37*) and NaY (*11*) zeolites. The EXAFS results are consistent with a mixture including roughly 80% of the Ir present in hexairidium clusters and the remainder present in iridium subcarbonyls.

The crystallographic data characterizing the salt of $[Ir_6(CO)_{15}]^{2-}$ indicate an Ir–C_t coordination number of 2, with an average distance of 1.86 Å, and an Ir–C_b coordination number of 1, with an average distance of 2.04 Å (*14*). The EXAFS data characterizing the supported iridium carbonyl are consistent with the crystallographic data characterizing $[Ir_6(CO)_{15}]^{2-}$. They indicate an Ir–C_t coordination number of 1.6 with an average distance of 1.82 Å and Ir–C_b coordination number of 0.8 with an average distance of 1.96 Å. However although the structural data characterizing the Ir–Ir, Ir–C_t, and Ir–C_b interactions agree well with the crystallographic data, the results characterizing the Ir–O* interaction (Table 3)

do not. The discrepancy between the Ir–C_t (1.6) and Ir–C_b (0.8) coordination numbers, which sum to 2.4, and the Ir–O* coordination number (1.8), which is expected to equal the sum of the two Ir–C coordination numbers, can be understood on the basis of multiple scattering effects (*31, 38*), as follows: The crystallographic distance between Ir and the O atoms of the terminal carbonyl ligands is virtually the same as the crystallographic distance between Ir and the O atoms of bridging carbonyl ligands. However, the Ir–C–O_t angle is 176.2°, whereas the Ir–C–O_b angle is 137.8° (*14*). When the Ir–C–O bond angle is greater than approximately 140°, the EXAFS phase shift and amplitude functions depend strongly on the positions of the atoms because of multiple scattering effects (*31, 38*). In contrast, the multiple scattering effect is not expected to be significant for bridging carbonyl oxygens in $[Ir_6(CO)_{15}]^{2-}$, since the Ir–C–O_b angle is only 137.8°. Since the terminal and bridging carbonyl oxygen atoms are located at nearly the same distance from Ir, it is difficult to separate the two contributions in the EXAFS analysis and to determine an accurate estimate of the overall Ir–O* coordination number. Consequently, we infer that the discrepancy between the sum of the Ir–C_t and Ir–C_b coordination numbers and the Ir–O* coordination numbers determined by the EXAFS data is a result of there being two types of carbonyl oxygen contributions at the same distance but experiencing different degrees of multiple scattering that lead to different phase shifts, which may give a negative interference and a low estimate of the Ir–O* coordination number.

In summary, the EXAFS data, in agreement with the infrared data, are consistent with the presence of $[Ir_6(CO)_{15}]^{2-}$ in the zeolite-supported iridium catalyst. The additional contribution may arise from unconverted $[Ir(CO)_2(acac)]$ or other mononuclear species. The results indicate that roughly 80% of the Ir atoms were present in the $[Ir_6(CO)_{15}]^{2-}$ clusters.

Formation and Stabilization of Iridium Carbonyl Clusters in NaX Zeolite

The evidence, based on the color, the infrared spectra, and the analogy to the chemistry of iridium carbonyls in basic solutions and on the basic MgO surface (*19*), indicates the formation of $[HIr_4(CO)_{11}]^-$ from $[Ir(CO)_2(acac)]$ at 75°C in NaX zeolite. The conversion of this cluster anion into $[Ir_6(CO)_{15}]^{2-}$ in the zeolite at 175°C is evidenced by the color, the infrared spectrum, and the EXAFS spectrum and is also consistent with the chemistry of iridium carbonyls in solution and on the MgO surface (*19*). Both the tetrairidium and the hexairidium cluster anions are stabilized by the CO ligands. The mechanisms of the transformations, even in solution, are not known. We might speculate that the conversion of the mononuclear iridium complex into the tetrairidium cluster anion involves reaction with CO and water (or hydroxyl groups) in the zeolite, since CO and water are reagents in the solution reaction; it seems likely that H^+ is produced in the zeolite, but there is no evidence for it.

The formation of anionic iridium carbonyl clusters in NaX zeolite is not surprising because NaX zeolite is relatively strongly basic. Evidence for the basicity of zeolite X containing alkali metal ions has been presented by several groups; the evidence is the catalytic activity for base-catalyzed reactions of hydrocarbons (*39*) and temperature-programmed desorption of adsorbed CO_2 (*40*). The nature of the basicity is not well understood; it may be associated with alkali metal oxides formed from alkali metal cations present in excess of the exchange cations. If H^+ were formed in the reduction of the iridium precursor to form the iridium carbonyl cluster anions, it would be expected to have reduced the basicity, but there are no data to determine the extent to which this may have occurred.

In contrast to the results reported here, however, the reaction in CO of $[Ir(CO)_2(acac)]$ on MgO initially gave

$[HIr_4(CO)_{11}]^-$, then $[Ir_8(CO)_{22}]^{2-}$, and then $[Ir_6(CO)_{15}]^{2-}$ (*19*). The yield of each of these cluster anions on MgO was high; specifically, under some conditions, virtually all of the iridium species were present as $[Ir_8(CO)_{22}]^{2-}$ on MgO (*19*). Since there was no evidence of the formation of the octairidium cluster in the NaX zeolite under the same conditions (or under any conditions observed in this work), we suggest that the confinement of the cages prevented its formation.

Similarly, neutral iridium carbonyl clusters are formed in acidic and neutral solutions (*13, 17*) and on the γ-Al_2O_3 surface (*20*). The cages of NaY zeolite, which have a relatively weak basic character, are also a medium for the synthesis of neutral iridium carbonyl clusters, namely, $[Ir_4(CO)_{12}]$ (*41, 42*) and two isomers of $[Ir_6(CO)_{16}]$ (*9, 11*). These results give an indication of the possibilities for modification of the reactivity in the solvent-like cages of the zeolites by changing the Si to Al ratio.

In summary, there is a parallel between the chemistry of the formation of iridium carbonyl clusters in solution, on metal oxide surfaces, and in zeolite cages.

Ion-Paring of Iridium Carbonyl Clusters with the NaX Zeolite Framework

The nature of the interactions between anionic metal carbonyls and alkali metal ions in solution (*43*) or on surfaces (*19*) has been the subject of investigations for years. Adduct formation between neutral metal carbonyls and Lewis acids, both in solution (*44*) and on surfaces (*45*), has also been investigated. Interaction of a metal carbonyl with alkali metal ions or with Lewis acids via the oxygen of a carbonyl group typically results in a large decrease of the infrared absorption frequency of the carbonyl group, with the stretching frequencies of the noninteracting carbonyl ligands all shifting to slightly higher frequencies.

A comparison of the spectrum of $[HIr_4(CO)_{11}]^-$ in NaX zeolite (Fig. 1B) with that of $[PPN][HIr_4(CO)_{11}]$ in THF (Table 2) shows a shift of the major terminal carbonyl band of the encaged species of about 15 cm^{-1} to higher frequency and a shift of the bridging carbonyl band of about 55 cm^{-1} to lower frequency. These shifts are consistent with ion pairing of $[HIr_4(CO)_{11}]^-$ with the Na^+ ions in the "solvating" zeolite cage, similar to the ion pairing of $[HIr_4(CO)_{11}]^-$ with the Mg cations on the MgO surface (*19*) and that of $[HIr_4(CO)_{11}]^-$ with Na^+ in diethyl ether (*30*). The relatively large shift of the bridging carbonyl band characteristic of NaX-supported $[HIr_4(CO)_{11}]^-$ suggests a strong interaction of the bridging carbonyl oxygen of the anion with Na^+ ions in the zeolite cage. Such an interaction is expected to result in a net electron withdrawal from the cluster, decreasing the backbonding to the terminal carbonyl ligands, strengthening the carbon–oxygen bonds, and shifting the terminal carbonyl bands to higher frequencies.

Similar trends in the infrared band shifts have been observed in the work with $[Ir_6(CO)_{15}]^{2-}$ in NaX zeolite (Fig. 1C). A comparison with the spectrum of $[PPN]_2[Ir_6(CO)_{15}]$ in THF and that of $[NEt_4]_2[Ir_6(CO)_{15}]$ in THF (Table 2) shows a shift of the major terminal carbonyl band of the encaged species of about 12 cm^{-1} to higher frequency and a shift of the bridging carbonyl band of about 60 cm^{-1} to lower frequency. Again, these results suggest ion pairing of $[Ir_6(CO)_{15}]^{2-}$ with the Na^+ in the zeolite cage.

Evidence of the Entrapment of Iridium Carbonyl Clusters in NaX Zeolite Cages

One of the main issues complicating the synthesis and characterization of metal clusters in zeolites is the possible simultaneous formation of metal clusters or crystallites outside the zeolite crystallites, which is apparently often virtually unavoidable. Much of the reported work with metal clusters and other nanostructures in zeolites has failed to include evidence to estab-

lish whether all the clusters were actually confined in the cages.

The results of the work summarized here are consistent with the inference that virtually all the iridium clusters were formed in and confined to the zeolite cages. The evidence is as follows:

(1) The synthesis conditions were chosen to remove iridium precursors and clusters from the outside of the zeolite crystals. The use of the neutral precursor [Ir $(CO)_2$(acac)] has the advantage of allowing removal of unconverted precursor that remained outside the crystallites by thorough washing with hexane; the infrared spectra indicate that the washing did not remove all the [Ir$(CO)_2$(acac)] from the sample. The results are consistent with the suggestion that the precursor that remained after the washing was inside the zeolite cages. Thus we infer that these precursors were the source of the iridium carbonyl clusters trapped in the zeolite cages.

(2) $[Ir_8(CO)_{22}]^{2-}$ is a dimer containing Ir_4 tetrahedra linked by an Ir–Ir bond; it has a length of about 15 Å, determined from the crystallographic data (*15*). This cluster is formed in the reductive carbonylation of iridium carbonyls in basic solutions and on strongly basic MgO surfaces. The lack of evidence of its formation during the reductive carbonylation of $[HIr_4(CO)_{11}]^-$ in the relatively strongly basic NaX zeolite is consistent with the suggestion that it is too large to fit in the zeolite supercage, which has a diameter of about 12 Å. The results give evidence that the zeolite-supported $[HIr_4(CO)_{11}]^-$ [with a diameter of about 9 Å, determined from the crystallographic data (*16*)] was trapped in the zeolite cages and directly transformed in the cages into $[Ir_6(CO)_{15}]^{2-}$, which has a diameter of about 11 Å [determined crystallographically (*14*)].

(3) Since $[HIr_4(CO)_{11}]^-$ and $[Ir_6(CO)_{15}]^{2-}$ are soluble in THF, the lack of extraction of these anionic carbonyl clusters from NaX zeolite with THF or with [PPN][Cl] in THF indicates that the anions were trapped in the zeolite cages, consistent with the fact that the clusters are too large to fit through the zeolite apertures. In contrast, the anionic iridium carbonyl clusters could be extracted from MgO, which has pores large enough to allow the rapid diffusion of the clusters. The lack of extraction of the clusters is the strongest evidence that they were trapped in the zeolite.

In summary, the results are consistent with a ship-in-a-bottle synthesis of the iridium carbonyl clusters. The precursor [Ir $(CO)_2$(acac)] is inferred to be small enough to fit into the interior of the zeolite, as similar, but larger, metal carbonyls have been shown to fit: $[CpM(CO)_2]$, $[Cp^*M(CO)_2]$ and $[CpM(C_2H_4)_2]$ [M = Rh, Ir; Cp = C_5H_5; Cp* = $(CH_3)_5C_5$] (*46*). Furthermore, $[HIr_4(CO)_{11}]^-$ and $[Ir_6(CO)_{15}]^{2-}$ are small enough to fit in the supercages of NaX zeolite but too large to diffuse rapidly through the apertures (which have diameters of about 7.4 Å). Therefore, the clusters, once formed, appear to be trapped in the supercages.

Stable and Selective CO Hydrogenation Catalyst

As shown in the preceding section, it is apparent that $[Ir_6(CO)_{15}]^{2-}$ was stable in the zeolite catalyst after being used in equimolar CO + H_2 at 20 atm for 1 day. The catalyst containing $[Ir_6(CO)_{15}]^{2-}$ is characterized by an unusual selectivity in CO hydrogenation; it gave a non-Schulz–Flory distribution of hydrocarbon products (with high yields of C_4 hydrocarbon), which contrasts with the Schulz-Flory distribution characteristic of alumina-supported Ir crystallites and virtually all conventional supported metal catalysts. Similar non-Schulz–Flory distributions have been observed with NaY-zeolite-supported catalysts containing osmium carbonyls (*6, 7*) and rhodium carbonyls (*8*) as well as with NaY-zeolite-supported catalysts containing $[Ir_6(CO)_{16}]$ (*11*). These results suggest that the precursors of the catalytically active

species in all these CO hydrogenation catalysts were metal carbonyl clusters trapped in the zeolite cages. The suggestion is based principally on the evidence that the catalysts containing the metal carbonyl clusters in zeolites are distinct from conventional supported metals in their selectivities. Other evidence is as stated by Zhou *et al.* (*7*). Thus, the results for a family of catalysts containing stable metal carbonyl clusters suggest that Muetterties' early speculation, referred to in the introduction, may have more validity than has been recognized. However, we caution that the identification of the catalytically active species in the zeolites remains uncertain, since small amounts of undetected and highly active species could also account for the observed catalytic behavior.

One might hope that the product distribution might provide some clues about the reaction mechanism and the nature of the catalytically active species. Except for the relatively high yields of the C_4 products, the product distributions are not unusual. High yields of C_3 and C_4 products have been observed before for zeolite-supported catalysts, but the explanation for the selectivities is not evident.

Pressure was found to be crucial for stable performance of the catalysts. The results show that a pressure of 20 atm maintained the catalytic performance for at least 1 day. These results indicate that the high pressure of CO is needed to maintain the carbonyl clusters during catalytic CO hydrogenation and thus maintain the catalytic performance. The stabilization of $[Ir_6(CO)_{15}]^{2-}$ in NaX zeolite during catalytic hydrogenation of CO is attributed to (1) the strength of the Ir–Ir bonds, (2) the CO ligands provided by the CO gas phase reactant, and (3) the geometry of the zeolite pores, with relatively large cages and small apertures which entrap the clusters and hinder their sintering into large, unselective Ir particles.

It has been shown that the used catalyst under a high H_2 partial pressure was black at the upstream end of the catalyst bed, suggesting that Ir metal particles had formed in or on the zeolite. We infer that under the high H_2 partial pressure, the zeolite-supported Ir carbonyl species were converted into metallic Ir. The product distribution data show that this catalyst behaved like a conventional supported metal catalyst, giving a Schulz–Flory distribution of hydrocarbon products. These results are consistent with the suggestion stated above that the catalytically active species in the more selective catalysts (those not exposed to high H_2/CO ratios) were iridium carbonyl species trapped in the zeolite cages. However, since the supported Ir metal crystallites are more active for CO hydrogenation than the catalyst that may have lacked them, it is not possible to exclude the possibility that the catalysis observed in the apparent absence of the metal should actually be attributed to small, undetected amounts of metal.

CONCLUSIONS

$[Ir(CO)_2(acac)]$ in the cages of NaX zeolite was converted in the presence of CO at 1 atm to $[HIr_4(CO)_{11}]^-$ at 75°C and to $[Ir_6(CO)_{15}]^{2-}$ at 175°C. The chemistry of these anionic carbonyl clusters is similar to that in basic solutions and on the basic MgO surface. The interactions of the clusters with the zeolite are explained by ion-pairing effects, indicated by the infrared spectra. The zeolite containing iridium carbonyls catalyzed the CO hydrogenation reaction at 20 atm and 250°C with a relatively high selectivity to C_4 hydrocarbons; it was stable for 3 days in a flow reactor and was reddish-brown when removed from the reactor. EXAFS and infrared spectra characterizing the used catalyst show that the predominant iridium species were $[Ir_6(CO)_{15}]^{2-}$, consistent with the inference that the entrapment in the zeolite supercages and the CO reactant stabilize the iridium clusters during the catalysis. The data are consistent with the suggestion that these cluster anions were the catalyst precursors, but the

possibility that small, undetected amounts of Ir metal were the actual catalytic species cannot be ruled out.

ACKNOWLEDGMENTS

We thank Professor D. C. Koningsberger of the University of Utrecht for many helpful discussions about EXAFS analysis. The EXAFS data were analyzed with the Eindhoven University EXAFS Data Analysis Program, developed by M. Vaarkamp and D. C. Koningsberger. This research was supported by the National Science Foundation (CTS-9300754). We also acknowledge the support of the U.S. Department of Energy, Division of Materials Sciences, under Contract DE-FG05-89ER45384, for its role in the operation and development of beam line X-11A at the National Synchrotron Light Source. The NSLS is supported by the Department of Energy, Division of Materials Sciences and Division of Chemical Sciences, under Contract DE-AC02-76CH00016. We are grateful to the staff of beam line X-11A for their assistance.

REFERENCES

1. Muetterties, E. L., *Bull. Soc. Chem. Belg.* **84,** 959 (1975).
2. Gladfelter, W. L., and Roesselet, K. J., *in* "The Chemistry of Metal Cluster Complexes" (Shriver, D. F., Kaesz, D., and Adams, R. D., Eds.), p. 329, VCH, Weinheim, 1990.
3. Chini, P., *Inorg. Chim. Acta Rev.* **2,** 31 (1968); Chini, P., *Pure Appl. Chem.* **23,** 389 (1970); Chini, P., Longoni, G., and Albano, V. G., *Adv. Organomet. Chem.* **14,** 285 (1976); Chini, P., *Gazz. Chim. Ital.* **109,** 225 (1979).
4. Lamb, H. H., and Gates, B. C., *J. Am. Chem. Soc.* **108,** 81 (1986); Lamb, H. H., Krause, T. R., and Gates, B. C., *in* "Proceedings, 9th International Congress on Catalysis, Calgary, 1988" (M. J. Phillips and M. Ternan, Eds.), Vol. 3, p. 1378. Chem. Institute of Canada, Ottawa, 1988.
5. Knözinger, H., and Gates, B. C., *in* "Metal Clusters in Catalysis" (Gates, B. C., Guczi, L., and Knözinger, H., Eds.), p. 531. Elsevier, Amsterdam, 1986.
6. Zhou, P.-L., and Gates, B. C., *J. Chem. Soc., Chem. Commun.* 347 (1989).
7. Zhou, P.-L., Maloney, S. D., and Gates, B. C., *J. Catal.* **129,** 315 (1991).
8. Lee, T. J., and Gates, B. C., *Catal. Lett.* **8,** 15 (1991).
9. Kawi, S., and Gates, B. C., *J. Chem. Soc., Chem. Commun.* 994 (1991).
10. Kawi, S., and Gates, B. C., *J. Chem. Soc., Chem. Commun.* 702 (1992).
11. Kawi, S., Chang, J.-R., and Gates, B. C., *J. Am. Chem. Soc.*, in press.
12. Mantovani, E., Palladino, N., and Zanobi, A., *J. Mol. Catal.* **3,** 285 (1977).
13. Angoletta, M., Malatesta, L., and Caglio, G. L., *J. Organomet. Chem.* **94,** 99 (1975).
14. Demartin, F., Manassero, M., Sansoni, M., Garlaschelli, L., and Martinengo, S., *J. Chem. Soc. Chem. Commun.*, 903 (1980).
15. Demartin, F., Manassero, M., Sansoni, M., Garlaschelli, L., Raimondi, C., Martinengo, S., and Canziani, F., *J. Chem. Soc. Chem. Commun.*, 528 (1981).
16. Bau, R., Chiang, M. Y., Wei, C.-Y., Garlaschelli, L., Martinengo, S., and Koetzle, T. F., *Inorg. Chem.* **23,** 4758 (1984).
17. Stevens, R. E., Lin, P. C. C., and Gladfelter, W. L., *J. Organomet. Chem.* **287,** 133 (1985).
18. Rode, E. J., Davis, M. E., and Hanson, B. E., *J. Catal.* **96,** 574 (1985).
19. Kawi, S., and Gates, B. C., *Inorg. Chem.* **31,** 2939 (1992).
20. Kawi, S., Chang, J.-R., and Gates, B. C., *J. Phys. Chem.*, in press.
21. van Zon, F. B. M., Ph.D. Thesis, Eindhoven University of Technology, The Netherlands, 1988; Maloney, S. D., Ph.D. Dissertation, University of Delaware, 1990.
22. Duivenvoorden, F. B. M., Koningsberger, D. C., Uh, Y. S., and Gates, B. C., *J. Am. Chem. Soc.* **108,** 6254 (1986).
23. Teo, B.-K., and Lee, P. A., *J. Am. Chem. Soc.* **101,** 2815 (1979).
24. Teo, B.-K., *J. Am. Chem. Soc.* **103,** 3990 (1981).
25. van Zon, J. B. A. D., Koningsberger, D. C., van't Blik, H. F. J., and Sayers, D. E., *J. Chem. Phys.* **82,** 5742 (1985).
26. Wyckoff, R. W. G., *in* "Crystal Structures," 2nd ed., Vol. 1, p. 10. Wiley, New York, 1963.
27. Trömel, M., and Lupprich, E., *Z. Anorg. Chem.* **414,** 160 (1975).
28. Churchill, M. R., and Hutchinson, J. P., *Inorg. Chem.* **17,** 3528 (1978).
29. Maloney, S. D., van Zon, F. B. M., Koningsberger, D. C., and Gates, B. C., *Catal. Lett.* **5,** 161 (1990).
30. Vandenberg, D. M., Choy, T. C., and Ford, P. C., *J. Organomet. Chem.* **366,** 257 (1989).
31. Maloney, S. D., Kelley, M. J., Koningsberger, D. C., and Gates, B. C., *J. Phys. Chem.* **95,** 9406 (1991).
32. Kirlin, P. S., van Zon, F. B. M., Koningsberger, D. C., and Gates, B. C., *J. Phys. Chem.* **94,** 8439 (1990).
33. van Zon, J. B. A. D., Koningsberger, D. C., van't Blik, H. F. J., and Sayers, D. E., *J. Chem. Phys.* **82,** 5742 (1985).
34. Koningsberger, D. C., and Prins, R., *in* "X-ray Absorption: Principles, Applications, Techniques of EXAFS, SEXAFS, and XANES" (D. C.

Koningsberger and R. Prins, Eds.), p. 395. Wiley, New York, 1988.
35. Tanaka, K., Watters, K. L., and Howe, R. F., *J. Catal.* **75,** 23 (1982).
36. Solymosi, F., Novak, E., and Molnar, A., *J. Phys. Chem.* **94,** 7251 (1990).
37. Kawi, S., and Gates, B. C., in preparation.
38. van Zon, F. B. M., Kirlin, P. S. Gates, B. C., and Koningsberger, D. C., *J. Phys. Chem.* **93,** 2218 (1989).
39. Hathaway, P. E., and Davis, M. E., *J. Catal.* **116,** 263 (1989).
40. Tsuji, H., Yagi, F., and Hattori, H., *Chem. Lett.* 1881 (1991).
41. Kawi, S., and Gates, B. C., *Catal. Lett.* **10,** 263 (1991).
42. Kawi, S., Chang, J.-R., and Gates, B. C., submitted for publication.
43. Darensbourg, M. Y., *Prog. Inorg. Chem.* **33,** 221 (1985).
44. Horwitz, C. P., and Shriver, D. F., *Advan. Organomet. Chem.* **23,** 219 (1984).
45. Tessier-Youngs, C., Correa, F., Ploch, D., Burwell, R. J. Jr., and Shriver, D. F., *Organometallics* **2,** 898 (1983).
46. Ozin, G. A., Haddleton, D. M., and Gil, C. J., *J. Phys. Chem.* **93,** 6710 (1989).